Available online at www.sciencedirect.com

ScienceDirect

Ceramics International 39 (2013) 8869–8875

CERAMICS INTERNATIONAL

www.elsevier.com/locate/ceramint

Influence of the preparation process on the electrical properties of high-field co-doped zinc oxide varistors

Geoffroy Gadacz[a,*], Sophie Beaudet-Savignat[a], Laurence Longuet[b], Jean-Louis Longuet[c]

[a]Laboratoire Céramiques et Composants Avancés, France
[b]Laboratoire Expertises Chimiques et Physicochimiques, France
[c]Laboratoire Microstructure et Comportement, CEA/DAM, BP 16, Monts Cedex 1, France

Received 15 November 2012; received in revised form 23 April 2013; accepted 24 April 2013
Available online 2 May 2013

Abstract

High-field ZnO/Bi_2O_3 varistors co-doped with Mn and Co were synthesized using a two-step co-precipitating process. A Zn^{2+} solution containing the Mn and Co doping elements was first precipitated into hydroxides, further converted into oxalates and finally calcined to create the doped ZnO phase. Bi^{3+} precipitated at the grain boundaries thanks to an HNO_3 treatment of the ZnO grains. The influence of the precursor type (nitrates or chlorides) and the calcination temperature on the properties of the powders and ceramics were investigated. ICP-AES, microstructural analysis and non-linear voltage measurements were used to characterize the samples. The type of precursor solution was found to have a strong influence on the electrical properties. Furthermore, the calcination temperature modified the microstructure of the powder and consequently also that of the varistor.

Keywords: Varistor; Soft chemistry; Precipitation; Zinc oxide; Bismuth oxide

1. Introduction

ZnO-like varistors were introduced more than forty years ago by Matsuoka [1]. Also known as voltage-dependant resistors, they have been widely studied because of their high and reversible non-linear *I–V* behavior [2–5]. Typically resistive at low voltages, they become conductive above a breakdown voltage. Their main characteristic is the breakdown field $E_{1.0A}$ taken at 1 A [6]. They are mainly used as transient surge suppressors or voltage regulators, and are especially useful for high voltage applications because of their tremendous surge energy absorption.

At the breakdown field, the *I–V* characteristic can be simulated by a power law given by the following equation:

$$I = KE^{\alpha} \quad (1)$$

where K is a proportional factor, α is the non-linearity coefficient, I is the current and E is the electric field. The higher the value of α, the greater is the non-linearity.

Varistors are generally composed of zinc oxide which is a nonstoichiometric n-type semiconductor with linear characteristics, and an additive considered as a varistor former (e.g. Bi_2O_3, Pr_2O_3, and Sb_2O_3) [7–10] added in quantities generally lower than 1 mol%. This varistor former is responsible for the non-linear effect and it is well accepted in the literature that it creates a highly resistive depletion layer at the grain boundaries, considered as a double Schottky barrier [11,12]. Different doping elements of the ZnO phase such as MnO_2, CoO, BaO, NiO or Al_2O_3 were studied in order to modify the non-linear characteristics [13–15] or improve the stability of the system [16–18].

These ceramics are usually prepared using an oxide mixing route, resulting in chemical inhomogeneities, strong dependence toward the characteristics of the raw materials (purity/granulometry), coarse microstructures and high sintering temperatures. Another drawback of this oxide mixing route is the insufficient homogeneity and stability of the grain boundaries.

During the course of this study, we elaborated ZnO/Bi_2O_3 sub-micrometric homogeneous varistor powders co-doped with Mn and Co using a soft chemistry process. We studied the

*Corresponding author. Tel.: +33 4 47 34 40 00.
E-mail address: ggadacz@gmail.com (G. Gadacz).

0272-8842/$ - see front matter © 2013 Elsevier Ltd and Techna Group S.r.l. All rights reserved.
http://dx.doi.org/10.1016/j.ceramint.2013.04.080

influence of two critical parameters of this process on the powders and the properties of the ceramics.

First, as the electrical properties of ZnO varistors are recognized to be very dependent of the content of impurities, we determined the influence of the precursor type (nitrate or chloride). Secondly, as it is well known that the physico-chemical properties of the final powder rely strongly on the decomposition temperature (modification of the specific surface area), its influence was also investigated.

2. Experimental procedure

The varistor powders had the following composition: 98.94 mol% ZnO, 0.25 mol% CoO, 0.25 mol% MnO and 0.56 mol% Bi_2O_3. Starting from Zn^{2+}, Mn^{2+} and Co^{2+} nitrates or chlorides (reagent grade), various aqueous solutions of precursor were prepared and titrated. The process was divided into two steps and conducted in the same manner for both precursor types. Zn^{2+}, Co^{2+} and Mn^{2+} salts were first mixed and homogenized according to the final composition. A saturated NaOH solution was added to simultaneously precipitate the Zn, Co and Mn hydroxides. After a period of vigorous mixing, a saturated oxalic acid solution was added to the reactor to convert the hydroxides into their corresponding oxalates. The resulting white precipitate was filtered, washed, dried, and calcined at 500 or 600 °C to obtain the combined ZnO powder. In a second step, the powder was mixed with an acidic aqueous $Bi(NO_3)_3$ solution. The mixture was again filtered, washed and dried before a second calcination step at 400 °C to decompose the bismuth nitrate.

Herein, the samples obtained from nitrates and chlorides are referred to as Ntr and Chl, respectively. The calcination temperature (500 °C or 600 °C) is also included to the sample references (e.g., Ntr-500 °C for the varistor prepared with nitrate and calcined at 500 °C).

Different analyses were carried out in order to characterize the powders, such as inductively coupled plasma-atomic emission spectrometry (ICP-AES, HORIBA Activa), servo-coulometric analysis for the determination of the content of chloride species, combustion analysis for the determination of N, O (LEICO TC-600) and H contents (HORIBA EMGA-621 W), X-ray diffraction (PANAnalytical X'Pert Pro with $K_\alpha(1)$ copper radiation) for phase identification, laser granulometry (Cilas granulometer), specific surface area measurements (Asap 2010 Micromeritics), thermogravimetric analysis (TGA, Setaram TAG 24) and scanning electron microscopy (SEM, ZEISS ULTRA Plus).

The powders were isostatically pressed at 100 MPa. The resultant slugs were sintered at 730 °C for 16 h—a temperature close to the theoretical eutectic temperature of the ZnO–Bi_2O_3 mixture [19]. This sintering temperature was chosen because a low temperature limits the grain growth and ensures that the breakdown field remains high. The relative densities of the slugs were measured using the Archimedes method, taking into account a theoretical density of 5.67 g/cm^3 for ZnO. Finally, the microstructures of the sintered compacts were examined using SEM.

Cylindrical pellets were cut into slugs. An Ag paste was deposited on both ends of the samples which were then calcined at 600 °C. A minimum of two varistors were tested for each composition.

3. Results

TGA measurements were carried out on the oxalate powders to ensure that their decomposition was complete for the two selected calcination temperatures. As shown in Fig. 1, the weight loss was identical for the samples prepared with nitrate and chloride. The decomposition was divided into two steps. First, the samples lost around 19% of their weight between 100 and 200 °C. This is typical of residual water desorption. Subsequently, the samples lost around 36% of their weight between 350 and 420 °C. A simple calculation led us to explain this weight loss as the oxalate decomposing into the corresponding oxide (e.g., ZnC_2O_4 into ZnO). These TGA analyses thus confirmed that the chosen firing temperatures of 500 and 600 °C led to a complete decomposition.

The purity of the final powders was determined using ICP-AES and combustion analysis (Table 1). The theoretical composition was respected for all the samples since the Zn,

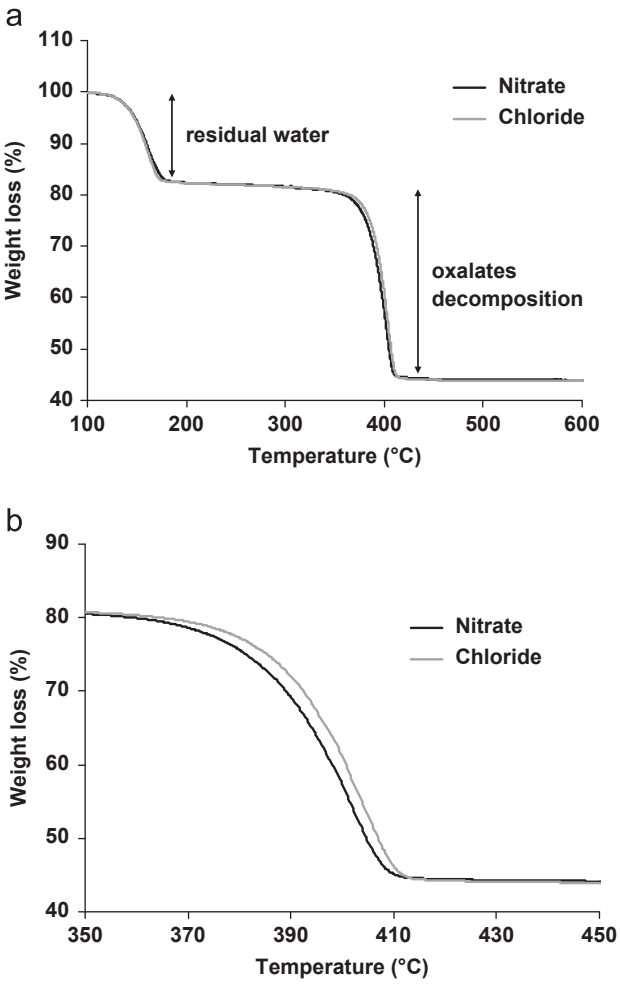

Fig. 1. (a) TGA analysis of nitrate and chloride prepared oxalates and (b) detail of the 350–450 °C range.

Table 1
ICP-AES measurements of the nitrate and chloride ZnO powders calcined at 500 °C and 600 °C.

Element	Ntr-500 °C (%)	Ntr-600 °C (%)	Chl-500 °C (%)	Chl-600 °C (%)	Theoretical
Zn	77.2 ± 3.9	77.2 ± 3.9	76.9 ± 3.8	76.4 ± 3.8	77.5
Bi	2.89 ± 0.14	2.80 ± 0.14	2.87 ± 0.14	2.72 ± 0.14	2.80
O	20 ± 2.0	21 ± 2.1	20.4 ± 2.0	20.10 ± 2.0	19.4
Co	0.17 ± 0.02	0.17 ± 0.02	0.17 ± 0.02	0.18 ± 0.02	0.18
Mn	0.17 ± 0.02	0.17 ± 0.02	0.17 ± 0.02	0.17 ± 0.02	0.16
	(ppm)	(ppm)	(ppm)	(ppm)	(ppm)
Na	84 ± 9	91 ± 18	77 ± 8	38 ± 4	0
Cl	< 20	< 20	< 20	< 20	0
H	855 ± 86	560 ± 56	855 ± 86	495 ± 50	0
N	< 20	180 ± 30	< 20	< 20	0

Mn, Co and Bi contents were within the error range for each preparation condition. Concerning the impurities, we noticed that some sodium remained in the samples. The highest quantity was reported for the Ntr-600 °C sample (91 ppm) and the lowest for the Chl-600 °C sample (38 ppm). Sodium had probably become trapped in the precipitates during the fast crystallization of the hydroxides. It was also found that the residual chloride content was low, proving that the washing procedure had been correctly performed, especially for the chloride synthesis. The hydrogen content appeared to be dependent on the calcination temperature. Its quantity was indeed higher for the two powders calcined at 500 °C (~850 ppm) than for the ones heat-treated at 600 °C (~500 ppm). This impurity probably originated from residual water adsorbed on solids or from residual hydroxides that did not fully decompose during the calcination. Finally, an unexplained high nitrogen content of 180 ppm was measured in the case of the Ntr-600 °C powder.

The scanning electron micrographs in Fig. 2 clearly show that the powders were composed of agglomerated round particles. Their apparent grain sizes depended on the calcination temperature: the two powders calcined at 500 °C (Fig. 2(a) and (c)) showed particle sizes around 50–80 nm, whereas the other two (Fig. 2(b) and (d)) had slightly larger particles around 100–150 nm. In order to confirm that these particles were dense, their specific surface areas were measured. Considering that the particles were perfectly spherical, it was possible to calculate their average diameter according to the following equation:

$$d = \frac{6}{\rho S_{BET}} \quad (2)$$

where d is the average particle diameter, ρ is the particle density (theoretically equal to 5.67 g cm^{-3}), and S_{BET} is the specific surface area obtained from the BET method.

Table 2 summarizes the BET results. As can be seen, the powders calcined at 500 °C had a higher specific surface area (around 15 m^2 g^{-1}) and a lower average particle size of 68 nm. In comparison, the powders calcined at 600 °C had a specific surface area around 8.5 m^2 g^{-1}, corresponding to a grain size of approximately 120 nm. These results were in good agreement with the SEM micrographs presented in Fig. 2, proving that the particles were dense and also that a significant grain growth occurred during the calcination between 500 °C and 600 °C.

It is also clear from Fig. 2 that all the powders are markedly agglomerated. The laser granulometry results (Fig. 3) confirm that the size of the agglomerates ranged between 0.5 μm and 10 μm. Except for the Chl-600 °C sample, all the powders had more or less the same particle size distributions.

Table 3 presents the results from the electrical characterizations and density measurements. The densities varied from one sample to another. The samples calcined at 500 °C were denser than those calcined at 600 °C. This can be easily explained by the particle sizes, which were initially smaller for the powders calcined at 500 °C, thereby inducing a higher sintering driving force. It was also visible that the varistors prepared with chloride were 10% denser than their nitrate counterparts. This result was difficult to explain as these powders had similar particle sizes, specific surface areas and impurity contents. The only possible explanation was a difference in the bismuth oxide distribution at the ZnO particle surface, inducing some local variations in the ZnO–Bi_2O_3 eutectic formation and a subsequent liquid phase sintering.

The breakdown voltage and α measurements showed very high breakdown fields, especially for the nitrate varistors. As can be seen in Fig. 3, the highest field was reported for the Ntr-600 °C sample (74.8 kV cm^{-1}) with a low α value of 22. A lower breakdown field value was obtained for the Ntr-500 °C sample (60 kV cm^{-1}) but with a much higher α in this case. The Chl-500 °C was impossible to measure due to the dielectric breakdown destroying the sample. Chl-600 °C presented a breakdown field of 42.9 kV cm^{-1} and an α value of 45.

In order to check the sample composition, X-ray diffraction analyses were performed. The results showed that only ZnO (Fig. 4(a)) and $Bi_{38}ZnO_{58}$ (Fig. 4(b)) were identified. According to the literature, this secondary phase (also known as $19Bi_2O_3$–ZnO) may be present at sintering temperatures above 738 °C [20] and is formed during the liquid phase sintering.

In order to estimate the breakdown field per grain boundary, a SEM overview was carried out (see micrographs in Fig. 5). The black regions correspond to the porosity, the gray ones to zinc oxide and the white ones to bismuth oxide. Compared to the ceramics prepared with chloride, those prepared with nitrate presented an inhomogeneous bismuth oxide repartition and a notable residual porosity, localized far from the bismuth oxide agglomerates. This result was in good agreement with the density measurements (Table 3). It was assumed that bismuth oxide was also poorly distributed in the initial nitrate-prepared powders, which may explain a less effective liquid phase sintering for these samples.

In a second step, the same SEM samples were chemically etched to reveal grain boundaries. As shown in Fig. 6, the grains were visible and a part of the bismuth oxide agglomerates remained present. The Chl-500 °C and Chl-600 °C samples appeared to have a similar ZnO grain size close to

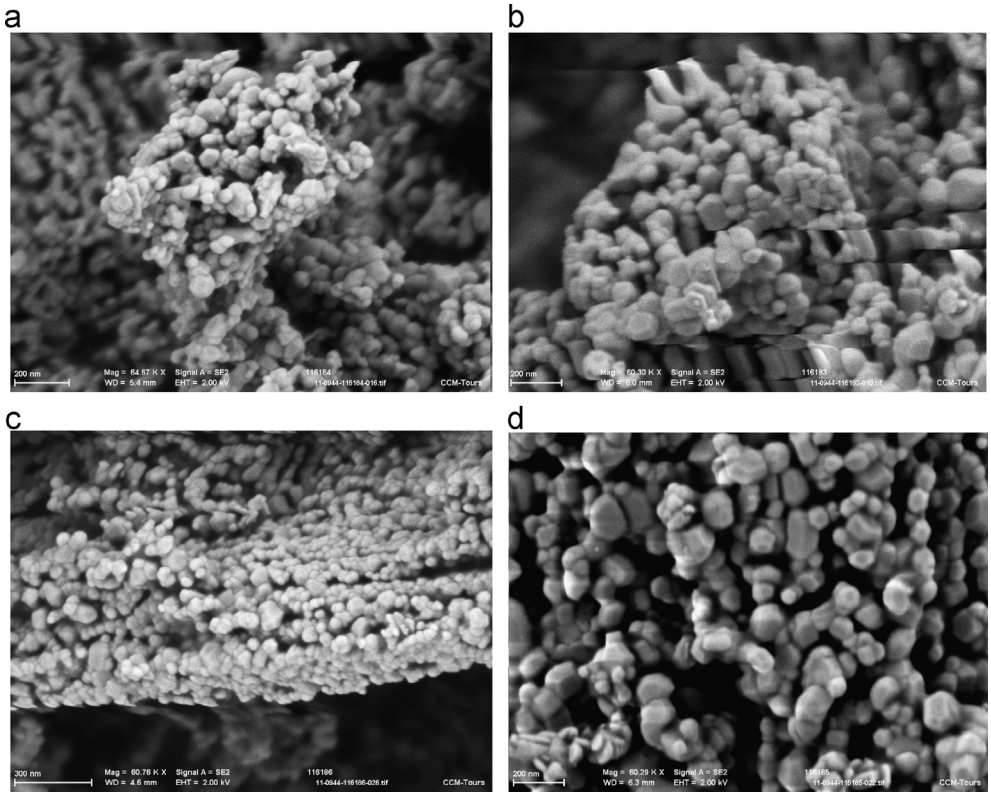

Fig. 2. SEM micrographs of the calcined ZnO powders: (a) Ntr-500 °C, (b) Ntr-600 °C, (c) Chl-500 °C, and (d) Ntr-600 °C.

Table 2
Specific surface area and calculated average grain size (obtained from Eq. (2)).

Sample (°C)	BET specific surface area ($m^2\ g^{-1}$)	Average grain size (nm)
Ntr-500	15.6	68
Ntr-600	8.5	124
Chl-500	15.5	68
Chl-600	8.8	120

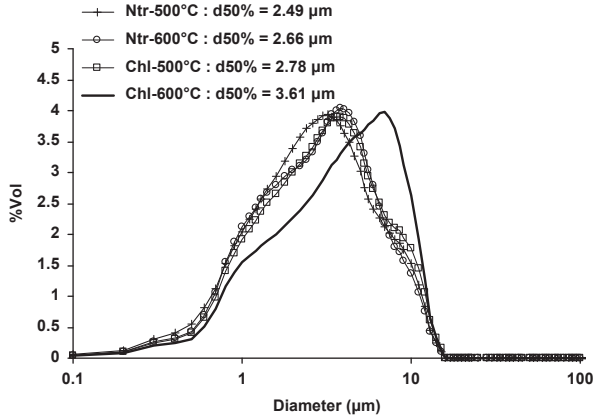

Fig. 3. Particle size distributions of the calcined powders.

1 µm, whereas the Ntr-600 °C and Ntr-500 °C samples had a different microstructure. Indeed, two sizes distributions can be observed on the micrographs. The first one was around 1 µm and the second one close to 0.5 µm. An estimation of the grain sizes was made using the intercept method (over 40 grains) based on several SEM observations and is summarized in Table 4, where it can be seen that the two studied parameters had an influence. The samples prepared with chloride presented a higher average grain size than their nitrate counterparts. It is difficult to explain why this parameter had such a notable effect. The chemical compositions were indeed identical and the powder characterizations showed no differences between the samples. According to the literature, the initial precursor type could have a significant impact on the sintering process but on a different kind of oxide ceramic [21]. The smaller grain size of the Ntr-600 °C and Nitr-500 °C samples can be explained by the role played by residual nitrogen as a grain growth inhibitor during sintering. Another explanation could be that the nitrogen increased the eutectic temperature of the ZnO–Bi_2O_3. However, further experiments need to be carried out to confirm this hypothesis.

Table 3
Densification and electrical properties of the varistor ceramics.

Sample (°C)	Relative density (%)	$E_{1.0A}$ (kV cm^{-1})	α
Ntr-500	80 ± 1	60 ± 1	45 ± 5
Ntr-600	78 ± 1	74.8 ± 1	22 ± 5
Chl-500	92 ± 1	Dielectric breakdown	Dielectric breakdown
Chl-600	89 ± 1	42.9 ± 1	45 ± 5

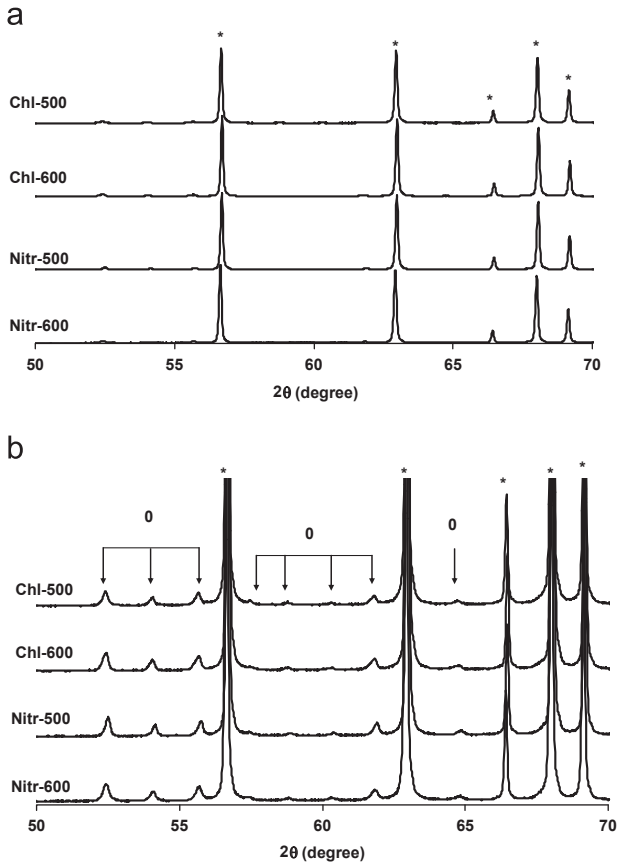

Fig. 4. X-ray diffraction analysis of the samples: (a) full-scale results and (b) zoomed results, '*' ZnO (JCPDS 01-070-8070) and '0' $Bi_{38}ZnO_{58}$ (JCPDS 00-042-0183).

Ntr-500 °C and Chl-500 °C samples presented larger grains than their Ntr-600 °C and Chl-600 °C counterparts. This can be explained by the higher specific surface areas of the powders calcined at 500 °C. The grain sizes of the powders were much smaller in this case, which probably increased their sintering reactivity.

Using this grain size estimation, it was possible to establish a relationship between the observed microstructures and the breakdown fields. Indeed, it is generally assumed that during the sintering process, an important drop in conductivity occurs on both sides of the grain boundary, known as the depletion layer. Since the grain boundaries are depleted of electrons, a voltage drop, typically between 2 and 4 V [5], appears upon application of an external voltage. Considering this system, it was possible to determine this voltage drop using the following equation:

$$V_g = \frac{E_{1.0\ \mathrm{A}}}{N_g} \tag{3}$$

where V_g is the voltage drop per grain boundary and N_g is the number of grains per cm. N_g was simply determined by dividing one by the corresponding average grain size obtained from the intercept method.

Based on the abovementioned SEM pictures, the voltage drop per grain estimated for each sample and (Table 4) confirmed the previous observations. The samples prepared with chloride presented larger grains than their nitrate counterparts. The sample Ntr-600 °C had the lowest average grain size (0.53 μm) associated to the highest breakdown field, compared with for instance the Chl-500 °C sample with the largest grains

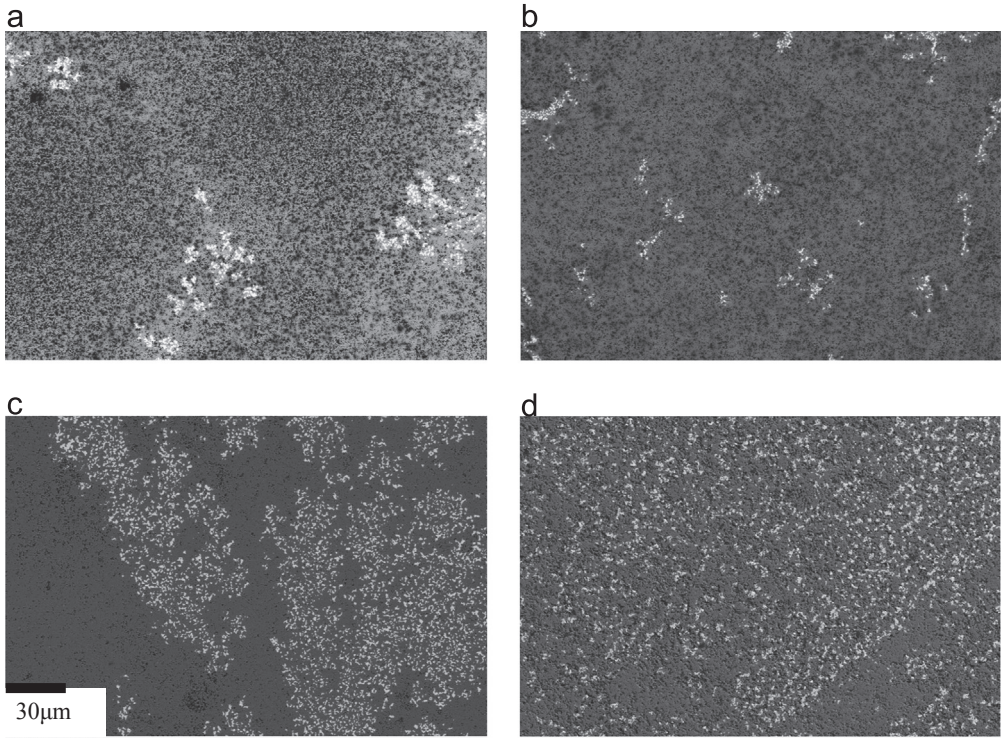

Fig. 5. SEM micrographs of the sintered samples : (a) Ntr-500 °C, (b) Ntr-600 °C, (c) Chl-500 °C, and (d) Chl-600 °C.

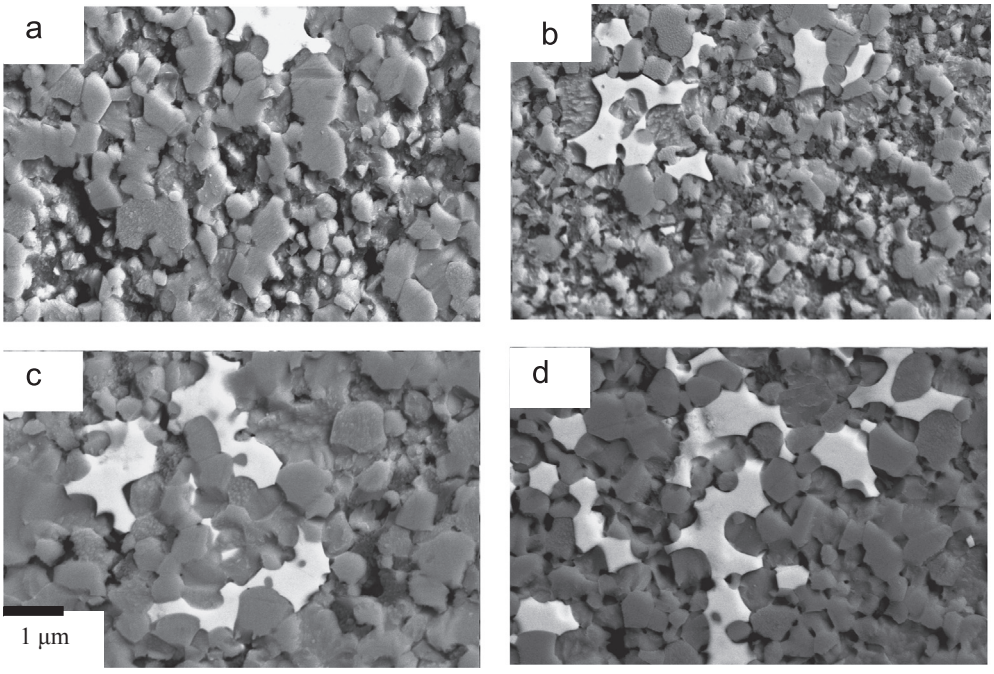

Fig. 6. SEM observations of the varistors after a surface chemical etching : (a) Ntr-500 °C, (b) Ntr-600 °C, (c) Chl-500 °C, and (d) Chl-600 °C.

Table 4
Average grain size and its relationship to the breakdown field.

Sample (°C)	Average grain size (μm)	$E_{1.0A}$ (kV cm^{-1})	E_g (V/grain)
Ntr-500	0.58	60	3.54
Ntr-600	0.53	74.8	3.96
Chl-500	1.00	Dielectric breakdown	–
Chl-600	0.87	42.9	3.73

(1 μm). The voltage drop per grain was nearly exactly the same for all the samples with values around 3.7 V, and also in the same order of magnitude as the results reported in the literature [22].

These average voltage drops prove that, despite different microstructures, the voltage barrier was not modified. In other words, the synthesis parameters (precursor type and calcination temperature) had a small influence on the barrier height. Furthermore, the bismuth oxide agglomerates observed in Fig. 5 did not significantly influence the final electrical results. This means that all the parameters studied here influenced the sintering process.

4. Conclusions

This paper has presented the influence of some critical parameters of a soft chemistry process used to elaborate the procedure for preparing zinc oxide varistors. Even if the different phenomena occurring during the synthesis are not fully understood, it was shown that the initial precursor had a strong influence on the final relative density and the microstructure of the ceramics. Effectively, ceramics prepared with chloride presented higher densities than their nitrate counterparts. These variations were partially explained by bismuth oxide homogeneity. The influence of the oxalate decomposition temperature was also studied and it was shown that by lowering the calcination temperature from 600 °C to 500 °C smaller powder particles were obtained. Finally, the correlation between the SEM micrographs and the breakdown fields rendered it possible to determine the average grain boundary breakdown voltage, which was similar from one sample to another, and in good agreement with the literature. This proved that the preparation conditions did not influence the barrier height or the breakdown voltage barrier, but strongly affected the sintering kinetics either by a modification of the grain growth speed or by an increase of the eutectic temperature of the ZnO–Bi_2O_3 system.

Acknowledgments

The authors wish to thank all the technicians and engineers who participated in this work.

References

[1] M. Matsuoka, Japanese Journal of Applied Physics 10 (1971) 736.
[2] G. Morris, Journal of Vacuum Science and Technology 13 (4) (1976) 926.
[3] J. Wang, W.G. Morris, American Ceramic Society Bulletin 53 (1974) 816.
[4] J. Wong, Journal of Applied Physics 47 (11) (1976) 4971.
[5] T.K. Gupta, Journal of the American Ceramic Society 73 (7) (1990) 1817.
[6] K. Mukae, et al., Japanese Journal of Applied Physics 16 (1977) 1361.
[7] K. Mukae, et al., Applied Physics Letters 50 (1979) 4475.
[8] L.M. Levinson, H.R. Philipp, Ceramic Bulletin 64 (1985) 639.
[9] M.A. Alim, et al., Journal of Applied Physics 63 (1988) 2337.
[10] D.R. Clarke, Journal of the American Ceramic Society 82 (1999) 485.

[11] A.B. Glot, Journal of Materials Science Materials in Electronics 17 (2006) 755.
[12] T.K. Gupta, Journal of Materials Science 20 (1985) 3487.
[13] A. Pandey, et al., Journal of Materials Science 19 (2008) 1122.
[14] W. Long, et al., Journal of the American Ceramic Society 93 (9) (2010) 2441.
[15] Z. Branković, et al., Ceramics International 27 (2001) 115.
[16] K. Yuan, et al., Journal of Alloys and Compounds 503 (2010) 507.
[17] M. Peiteado, et al., Ceramics International 37 (2011) 819.
[18] S.L. Jiang, et al., Journal of Electroceramics 21 (2008) 528.
[19] J.P. Guha, et al., Journal of Materials Science 39 (2004) 911.
[20] J.H. Hwang, et al., Journal of the American Ceramic Society 77 (1994) 1499.
[21] N. Roussel, et al., Ceramics International 37 (2011) 3565.
[22] M. Tao, et al., Journal of Applied Physics 61 (4) (1987) 1562.